

Affinity-mediated sorting order reversal of single-walled carbon nanotubes in density gradient ultracentrifugation

This content has been downloaded from IOPscience. Please scroll down to see the full text.

2016 Nanotechnology 27 41LT01

(<http://iopscience.iop.org/0957-4484/27/41/41LT01>)

View [the table of contents for this issue](#), or go to the [journal homepage](#) for more

Download details:

IP Address: 165.132.31.39

This content was downloaded on 06/09/2016 at 02:55

Please note that [terms and conditions apply](#).

Letter

Affinity-mediated sorting order reversal of single-walled carbon nanotubes in density gradient ultracentrifugation

Myungsu Jang, Somin Kim, Haneul Jeong and Sang-Yong Ju

Department of Chemistry, Yonsei University, 50 Yonsei-ro, Seodaemun-Gu, Seoul 03722, Korea

 E-mail: syju@yonsei.ac.kr

Received 6 July 2016, revised 7 August 2016

Accepted for publication 19 August 2016

Published 7 September 2016



CrossMark

Abstract

Sorted single-walled carbon nanotubes (SWNTs) are of paramount importance for their utilization in high-end optoelectronic applications. Sodium cholate (SC)-based density gradient ultracentrifugation (DGU) has been instrumental in isolating small diameter (d_t) SWNTs. Here, we show that SWNTs wrapped by flavin mononucleotide (FMN) as a dispersing agent are sorted in DGU, and show sorting order reversal behavior, departing from prototypical SC-SWNT trends. Larger d_t SWNTs are sorted in lower density (ρ), and buoyant ρ distribution of FMN-SWNT ranges from 1.15–1.25 g cm⁻³. Such a nanotube layering pattern originates from both the binding affinity between FMN and SWNT and the less-susceptible hydrated volume of remote phosphate sidechains of FMN according to nanotube d_t change.

 Online supplementary data available from stacks.iop.org/NANO/27/41LT01/mmedia

Keywords: single-walled carbon nanotube, separation, density gradient ultracentrifugation, buoyant density, binding affinity

(Some figures may appear in colour only in the online journal)

1. Introduction

Single-walled carbon nanotubes (SWNTs), indexed by (n, m) vectors, have excellent optoelectronic properties and are useful for various applications such as high-performance field-effect transistors [1–4] and photovoltaic cells [4–7]. However, since they are typically produced in a highly agglomerated and heterogeneous form, the separation of SWNTs according to chirality and electronic type via a solution process enables their low-cost widespread application.

Among various separation methods developed so far [8–15], the sodium cholate (SC)-based density gradient ultracentrifugation (DGU) scheme [8, 9, 16–18] using iodixanol has been instrumental to producing pure SWNTs according to electronic type [8, 19], chirality [8, 17, 20, 21], handedness [17, 18], and length [11, 22]. In this method, SC creates differently assembled configuration and

compactness on different SWNT electronic types [23], and the resulting SC-SWNTs with different buoyant density (ρ) assembly migrate to regions of like density. This method enables smaller diameter (d_t) SWNT sorting of less than 1 nm, due to a larger hydrate volume difference. The sorting order of SWNTs can be marginally controlled via pH [8, 24], and co-surfactant [8, 17, 21]. On the other hand, since larger d_t SWNTs have a relatively smaller hydrate volume difference, the DGU method results in only electronic-type enrichment having various chiralities [8, 19]. Therefore, a novel dispersing agent in DGU is necessary to isolate larger d_t SWNT chirality, which has shown superior electronic performance [25], and to attain controlled sorting according to SWNT d_t distribution.

In the meanwhile, flavin mononucleotide (FMN, figure 1(A)) is an individual wrapping agent for nanotubes in a helical pattern [26–28]. The FMN-SWNT displays distinct binding affinity (K_a) according to nanotube chirality [11, 29] via optical titration assay. In particular, the similar affinity of

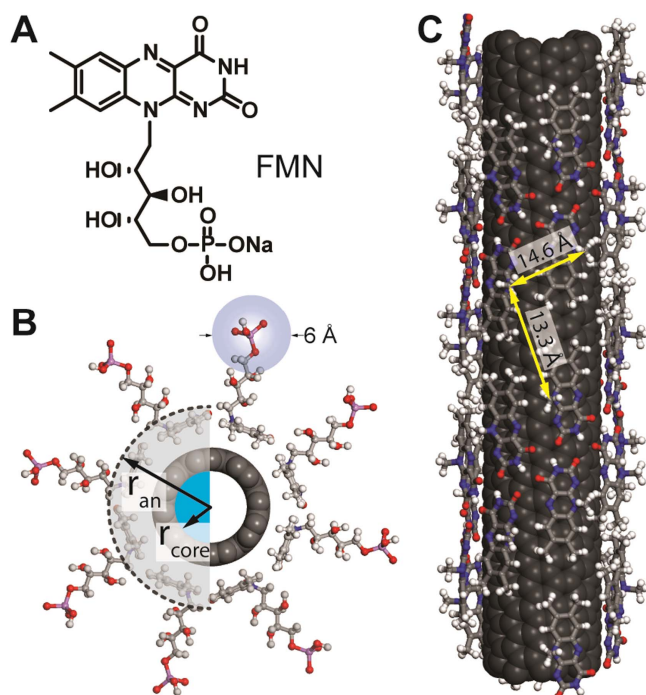


Figure 1. (A) Chemical structure of FMN. (B) Top and (C) side views of helical wrapping of FMN on SWNTs. Anhydrous radius r_{an} , and core radius r_{core} are illustrated. *d*-ribityl phosphate groups in (C) are eliminated for visual clarity. Distances indicated by yellow lines are from adjacent phosphate moieties.

FMN with SC toward SWNTs [29] suggests that FMN might be an alternative to SC derivatives of the DGU sorting method. As evidenced by transmission electron microscopy (TEM) [11] and atomic force microscopy (AFM) [28], the distinct hydrophilic *d*-ribityl phosphate tethered to hydrophobic isoalloxazine moieties of the FMN helical assembly on SWNTs may serve as a simple model to control the resulting hydrated volume, as shown in figure 1(B).

In this study, we find that SWNTs wrapped by FMN are sorted according to their chiralities in DGU, and their sorting order does not follow the prototypical d_t -dependency with increasing ρ which is observed in SC or DNA [9]-based DGU. A custom-made photoluminescence excitation (PLE) profiling setup allows us to probe SWNT photoluminescence (PL) along the centrifuge tube, showing larger d_t tubes positioned in lower ρ . Such sorting mainly originates from the K_a difference of various SWNTs with FMN, probed by an optical titration assay with a co-surfactant. The assay reveals that FMN has larger K_a with larger d_t SWNTs, and exhibits the K_a tendency matching with the sorting order according to nanotube chirality. Also, remote phosphate groups from the SWNT surface cause invariant hydrated volume with decreasing d_t and result in SWNT sorting order reversal.

2. Experimental section

Flavin mononucleotide (FMN, 73%–79%, Cat. No. F6750) and sodium dodecyl benzene sulfonate (SDBS, technical grade, Cat. No. 289957) were purchased from Sigma-Aldrich.

Deionized water (H_2O , spectroscopic grade, Cat. No. 19391) was obtained from Alfa Aesar and used as received. SWNTs prepared by a high-pressure carbon monoxide process (HiPco [30], raw grade, Batch #R1-831, d_t distribution of 1.00 ± 0.35 nm) were purchased from Nanointegris. Iodixanol (OptiPrep™, 60 w/v% in water, density of 1.320 ± 0.001 g ml⁻¹) was purchased from Axis-shield. UV–vis–near-infrared (NIR) absorption spectra were measured with a Cary 5000 spectrometer. Cuvettes with a path length of 10 mm were used throughout this study. Refractive indices (n_D) of density gradient solutions were measured using the NAR-2T Abbe refractometer equipped with a sodium D line light source at 22 °C. About 0.1 ml of the sample was placed between the primary and secondary prisms in the refractometer. The refractive index was obtained by measuring the critical angle (θ_c) of the media. θ_c was converted to refractive index (n_D) using the following equation: $n_D = 1/\sin \theta_c$. The procedures and instrumentation used in this research are described in more detail in the online supplementary information.

3. Results and discussion

An FMN-SWNT dispersion sample for DGU was prepared as follows. An individualized sample was prepared by sonicating a mixture of 7.5 mg HiPco and 150 mg FMN (1 weight per volume %) in 15 ml of H_2O for 5 h, followed by 80 kg ($g = 9.8$ m s⁻²) ultracentrifugation (see Methods in the online supplementary information), modified from the previously established methods [11, 29]. This modification leads to increased SWNT dispersion. The resulting absorption spectrum and PLE map (figures 2(A) and (B), respectively) show distinct vis–NIR peak features originating from FMN-SWNT chiralities. Both spectra show that the first optical transition (E_{11}) region of SWNTs from 950–1350 nm is well-resolved with multiple peaks which originate from (n, m) chirality [31], which is in agreement with the PL positions of FMN-HiPco [11]. Further analysis of the PLE map shows that the dominant SWNT chiralities are (6,5), (7,5), (8,4), and (8,6) species in that order (17%, 15%, 14%, and 12%, respectively, see figure S1 of the online supplementary information for their abundance histogram). Using this sample, DGU with a nonlinear density iodixanol gradient was performed.

Figure 2(C) displays photographs of the centrifugation tube before and after ultracentrifugation at 80 kg for 20 h in the presence of the as-dispersed FMN-SWNTs. In order to ensure the colloidal stability of SWNTs, 1 mM FMN, evident by the yellow color of the centrifuge tube, was added to throughout the iodixanol gradient, which was carefully stacked with different ρ from 1.107–1.320 g cm⁻³ (see Methods and table S1 in the online supplementary information). After a gradient equilibrium period in tilted configuration for 1 h, the prepared nonlinear density along the centrifugation tube (figure 2(D)) was determined by measuring refractive indices of each layer via a refractometer and subsequent linear correlation with density (see Methods for

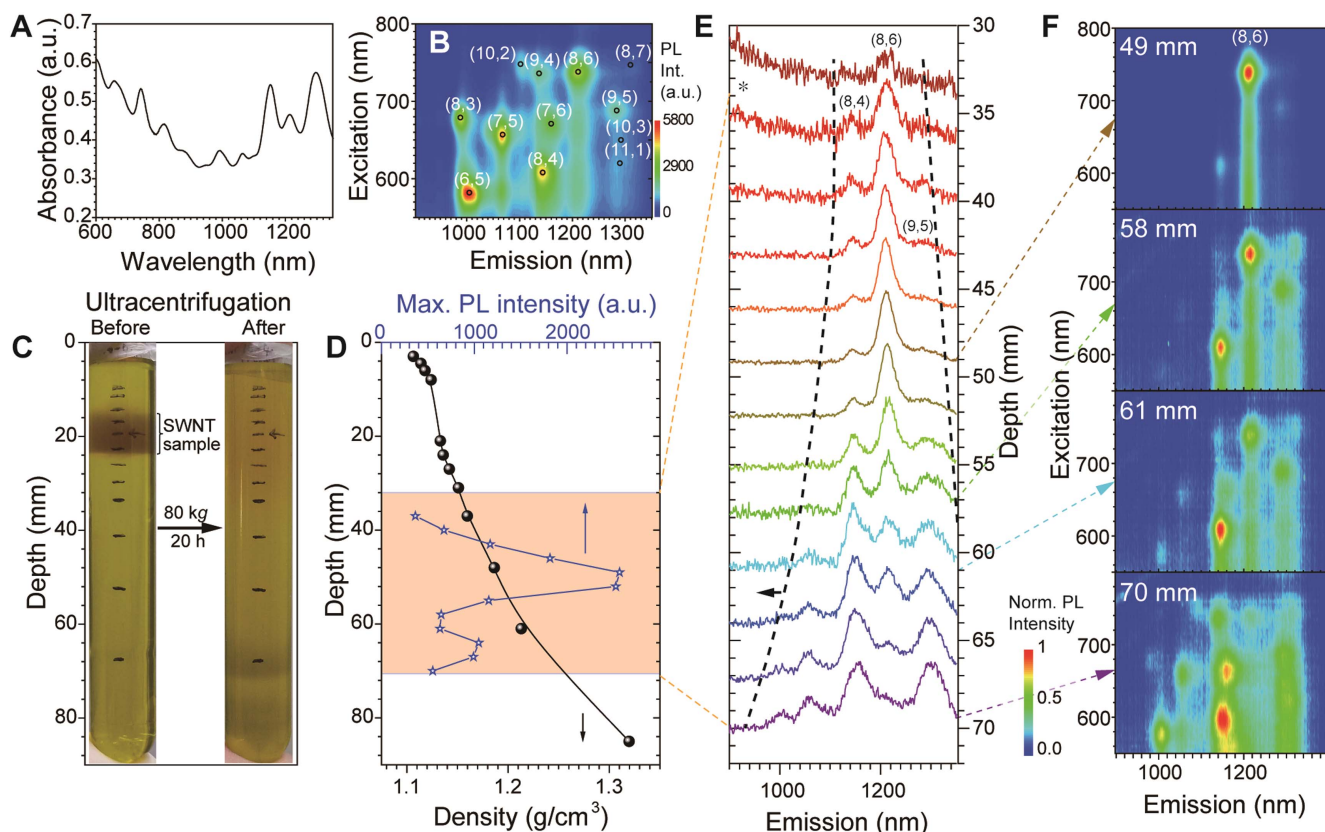


Figure 2. Chirality enrichment of FMN-dispersed SWNTs after the nonlinear DGU process. (A) Vis–NIR absorption spectrum and (B) PLE map of the FMN-dispersed SWNT sample. (C) Photographs of the nonlinear DGU tube containing FMN-SWNTs before and after the ultracentrifugation step. (D) Maximum PL intensity profile of SWNTs as a function of the tube depth (or density). (E) Normalized PL emission spectra measured at 3 mm intervals along the tube depth. Asterisks indicate PL tailing originating from FMN. Dotted lines indicate increased kinds of SWNTs. (F) The corresponding PLE maps from the selected depths.

measurement details, and online supplementary figure S2 for the correlation plot between the refractive indices and resulting densities). 1 ml of FMN-SWNT mixed with 25 w/v % iodixanol solution was cautiously loaded in the isopycnic position of the centrifugation tube (marked region in figure 2(C)). After 80 kg ultracentrifugation, the tube showed the successful disappearance of the initial FMN-SWNT loading bands and the gradually increased optical density with increasing depth up to 71 mm.

A custom-made translation stage equipped in a sample chamber of the PLE spectrometer allows us to probe the SWNT PL spectra in the centrifuge tube at 3 mm intervals along the depth, probed by 1 mW 635 nm laser (see Methods and figure S3 of the online supplementary information for the photograph of the actual optical setup). PL intensities from FMN-SWNTs were observed at ρ ranging from 1.15–1.25 g cm⁻³. This ρ range is rather heavier than those of SC-SWNTs (i.e. 1.05–1.11 g cm⁻³) [17] and DNA-SWNTs (i.e. 1.11–1.17 g cm⁻³) [9] although they utilize similar nanotube d_t distribution. The buoyant density of surfactant-SWNTs is controlled by contributions from the layered structure of hydrated, anhydrous, and core parts, as illustrated in figure 1(B). In a simple cylindrical geometric model, the buoyant density is explained by the following equation

[32, 33] :

$$\begin{aligned} \rho_{\text{buoyant}} &= \frac{\rho_{\text{anhydrous}} V_{\text{anhydrous}} + \rho_{\text{hydration}} V_{\text{hydration}} + \rho_{\text{core}} V_{\text{core}}}{V_{\text{anhydrous}} + V_{\text{hydration}} + V_{\text{core}}} \\ &= \frac{\rho_{\text{anhydrous}} (r_{\text{an}}^2 - r_{\text{core}}^2) + \rho_{\text{hydration}} (r_{\text{b}}^2 - r_{\text{an}}^2) + \rho_{\text{core}} r_{\text{core}}^2}{r_{\text{b}}^2} \end{aligned} \quad (1)$$

where, r_{b} , r_{an} , and r_{core} denote effective hydrated radius, anhydrous radius, and core radius, as illustrated in figure 1(B). Assuming that the core density of water remains equal to the average density of the surfactant solution (1.00 g cm⁻³) [32, 33], the parameters considered for the buoyant density calculation are anhydrous and hydration densities and their radii. This initially suggests that FMN on SWNT might have either lower hydration volume or higher anhydrous volume, as indicated in figure 1(B). The gray band observed from 74 mm to the tube end originates from non-fluorescent bundled SWNTs, checked by PLE maps (data not shown).

SWNT chirality distribution along the tube depth was compared by using PL emission spectra (figure 2(E)). In depths from 34–52 mm, preferential (8, 6) chirality enrichment with 1210 nm emission is confirmed, along with minor constituents such as (8, 4) and (9, 5) tubes with 1148 and 1282 nm PL, respectively. PL emission spectra of the region

from 55–70 mm indicate that, while the PL intensity of (8, 6) chirality decreased with increasing depth, other (n, m) chiralities increased their PL intensities at higher ρ (guided by dotted lines).

Since the PL emission spectra probed by the single excitation provide only qualitative information on (n, m) chiralities, PLE maps obtained at 3 mm intervals were acquired as shown in figure 2(F) (see figure S4 of the online supplementary information for the full ten PLE maps along the tube depth). As shown in the top PLE map, (8, 6) population is the most enriched at lower ρ (i.e. 1.15–1.18 g cm⁻³ or 49 mm) with 62% purity based on PL (figure S5 of the online supplementary information for relative enrichment along the depth based on PLE maps). The measured ρ is slightly lower than the calculated anhydrous density of FMN with the (8, 6) tube (i.e. 1.22 g cm⁻³, see Methods for the density calculation). The small difference between the buoyant density and calculated anhydrous density suggests that the hydrated volume contribution to buoyant density is quite small [32, 33]. In addition, there are minor constituents such as (8, 4) and (9, 5) nanotubes with 13.7% and 8.5% abundances, respectively. Smaller d_t SWNTs are enriched at higher ρ region (i.e. 1.18–1.25 g cm⁻³). It appears that SWNT population other than (8, 6) gradually increases with increasing ρ . The PLE maps acquired at 58 mm display increased enrichment of (8, 4) and (9, 5) species (by 24.6% and 14.4%, respectively), along with minor PL from (11, 1), (10, 3), (7, 6), and (8, 7). With further increasing ρ , the PLE maps display much broader SWNT distributions with decreasing (8, 6) PL.

Interestingly, (8, 6), (9, 5), and (8, 4) tubes situated at low ρ possess relatively larger $d_t > 0.8$ nm (based on 1.42 Å C-C distance) among HiPco, and previously showed higher K_a values determined by the optical titration method [11, 28, 29]. Optical titration is a unique way to determine K_a between FMN-SWNT chiralities by titrating SDBS, which replaces FMN wrapping on SWNTs at increasing concentration, and induces the PL intensity changes of the SWNTs. Since K_a between FMN and SWNTs varies according to temperature and FMN concentration [29], we measured K_a at 293 K (see Methods in online supplementary information) [11, 28, 29]. Figures 3(A)–(C) show three PL traces of representative FMN-SWNTs (i.e. (8, 6), (9, 5), and (8, 4)) replaced by SDBS. The PL intensity exhibits sigmoidal changes, which can be described by a Hill equation as following:

$$PL_{\text{SDBS}} = \frac{[\text{SDBS}]^\gamma}{[K_a]^\gamma + [\text{SDBS}]^\gamma}. \quad (2)$$

where K_a is defined as the SDBS concentration required to produce half the maximum PL intensity of specific (n, m) chirality with SDBS wrapping, PL_{SDBS} is PL intensity measured at the SDBS position of each nanotube, and γ is the fitted Hill coefficient describing the breadth of the sigmoidal transition and cooperativity of the co-surfactant [29]. The K_a values of FMN to (8, 6), and (9, 5) tubes are 0.68 ± 0.004 , 0.72 ± 0.0004 mM, respectively. Interestingly, (8, 4) tubes are best described with two K_a at 0.49 ± 0.004 and 0.72 ± 0.0004 mM, which might originate from two optical

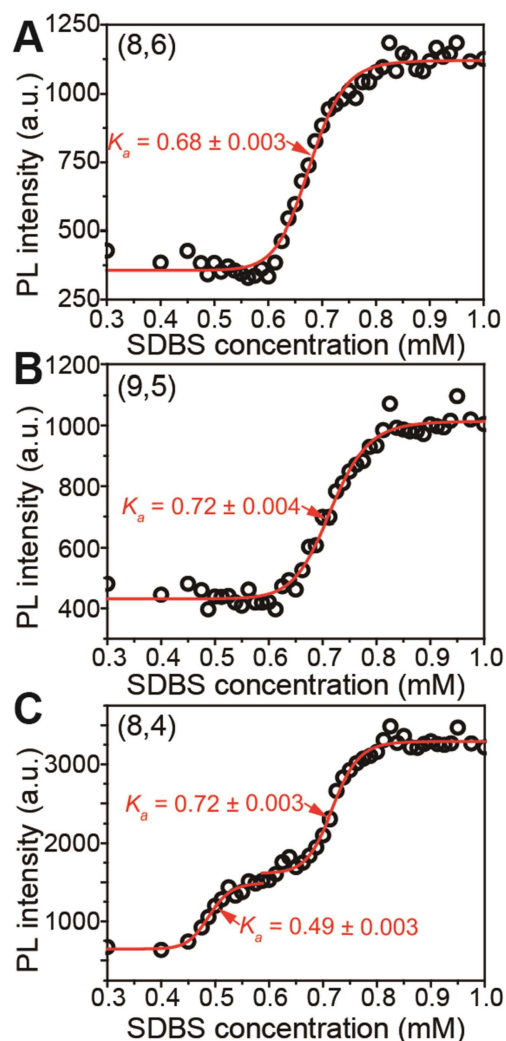


Figure 3. K_a determination by titrating FMN-SWNT against SDBS according to nanotube chiralities from (A) (8, 6), (B) (9, 5), and (C) (8, 4) PL positions. Black circle denotes PL intensities from the SDBS-SWNT.

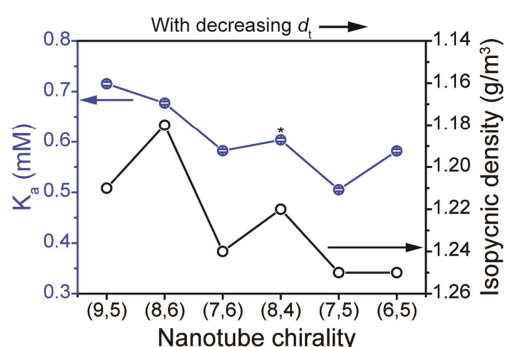


Figure 4. Comparison of K_a values (blue circle) with error bars with isopycnic densities (black circle) of FMN-SWNT according to SWNT chirality. The asterisk indicates average point of two K_a values.

SWNT isomers interacting differently with chiral FMN [26]. Overall, K_a of the larger d_t tubes with FMN are larger than the observed smaller d_t (n, m) tubes and are listed in table S2 of the online supplementary information.

Figure 4 shows the K_a value and the isopycnic density patterns according to nanotube chirality with decreasing d_t . First, the K_a generally decreases with decreasing d_t . The reason that the FMN helical assembly has the highest K_a with larger d_t nanotubes such as (8, 6) and (9, 5) is due to its optimal self-assembly diameter with underlying SWNTs [11]. The isopycnic density trend according to nanotube chirality roughly decreases as well, and exhibits large fluctuation in ρ . Interestingly, deviating SWNT species (i.e. (8, 6) and (8, 4)) from the decreasing density trend with decreasing d_t coincide with those from the K_a pattern. This indicates that binding affinity plays a role for FMN-based nanotube sorting in DGU. We speculate that the above preferential sorting of the (8, 6) tube in DGU compared to the (9, 4) and (8, 4) tubes originates from the higher stability of the FMN-(8, 6) tube, along with the initial chirality abundance in online supplementary figure S1 [11, 29, 28]. In fact, there is a dynamic equilibrium between free FMN and FMN on SWNTs. Since DGU media contain less FMN (i.e. 1 mM), this might cause a slight shift of equilibrium from higher FMN to lower FMN on SWNTs. Therefore, during the ultracentrifugation step, the FMN-SWNT might form bundles due to higher g force and the tube with higher K_a would survive. Considering the initial abundance and FMN-SWNT stability, this could lead to preferential (8, 6) enrichment. Overall, this sorting tendency is in stark contrast to the previous sorting tendency of SC-dispersed SWNTs, which showed progressively smaller d_t nanotubes placed at low ρ [8].

The question raised is why nanotubes with larger d_t migrate to low ρ . According to a simple, geometric model treating a nanotube as a hollow cylinder, the intrinsic mass per volume of a nanotube is expected to vary inversely with d_t [9]. However, in the case of SC- or DNA-based DGU sorting, the ratio of external hydrate volume to the volume of a bare nanotube is known to decline with increasing nanotube d_t . This is due to the lesser hydrated volume of the larger d_t surfactant–nanotube, compared to those from smaller d_t ones. However, we need to point out that this trend is not general and the structural factor of dispersing agents should be considered as well. SC has hydrophilic parts consisting of three hydroxyl groups and carboxylate in close proximity to adjacent SC molecules, as shown in online supplementary figure S7 [32]. Therefore, it is expected that smaller d_t SWNT would expose hydrophilic parts of SC to exterior water.

In our case, FMN has three distinct parts: nanotube-interacting isoalloxazine, and d -ribityl linker, and remote anionic phosphate groups, as shown in figure 1(A). d -ribityl and phosphate moieties determined by nuclear magnetic resonance (NMR) relaxation [34] and x-ray crystallography [35] studies directly interact with 1.2 and 6–18 water molecules, respectively. This suggests that the phosphate group is an effective contributor to the hydrate volume of FMN-SWNTs. Such a water cluster is estimated to form a single shell around phosphate with a diameter of 6 Å (figure 1(B)). The nearest phosphate distances along near longitudinal and radial directions, based on the atomistic energy minimized model of FMN on (8,6) [11, 26], are about 13.3 and 14.6 Å,

respectively, as shown in figure 1(C). With smaller d_t nanotubes, the longitudinal distance between phosphates is not affected due to the nearly fixed δ_1 helix pattern in figure 1 C [11]. Therefore, smaller d_t tubes only reduce the near radial distance between phosphates (for example, 11.5 Å for (6, 5) tube with $d_t = 0.75$ nm) to a small extent and, therefore, do not affect the hydration volume of phosphate much, due to close contact. As a result, the smaller hydrated volume of the remote phosphate group provides the buoyant density of the FMN-SWNT invariant with d_t change and the intrinsic mass per volume change governs the sorting behavior. This qualitatively explains why FMN-SWNTs exhibit sorting order reversal with d_t .

4. Summary

In brief, we found that FMN enables SWNT sorting order reversal in the DGU method. A custom-made setup allows us to probe SWNT PL along a centrifugation tube, showing a larger d_t nanotube in lower density. FMN affinity towards SWNT distorts the buoyant density of the resulting surfactant-SWNT. Also, the remote phosphate group of FMN is less prone to hydrated volume change with nanotube d_t variation. The combination of FMN with SC as a mixed surfactant will be useful to overcome smaller d_t -specific sorting. This FMN-based SWNT sorting in DGU will be a useful method to sort large d_t SWNT handedness and length, along with the layer sorting of graphene.

Acknowledgments

This research was supported by the Basic Science Research Program through the National Research Foundation of Korea (NRF) funded by the Ministry of Education, Science, and Technology (2014R1A1A2055572) and in part by the Yonsei University Future-Leading Research Initiative of 2014 (2014-22-0123).

References

- [1] Franklin A D 2013 Electronics: the road to carbon nanotube transistors *Nature* **498** 443–4
- [2] Franklin A D, Luisier M, Han S-J, Tulevski G, Breslin C M, Gignac L, Lundstrom M S and Haensch W 2012 Sub-10 nm carbon nanotube transistor *Nano Lett.* **12** 758–62
- [3] Wang C, Zhang J, Ryu K, Badmaev A, De Arco L G and Zhou C 2009 Wafer-scale fabrication of separated carbon nanotube thin-film transistors for display applications *Nano Lett.* **9** 4285–91
- [4] Wang H *et al* 2014 High-yield sorting of small-diameter carbon nanotubes for solar cells and transistors *ACS Nano* **8** 2609–17
- [5] Arnold M S, Zimmerman J D, Renshaw C K, Xu X, Lunt R R, Austin C M and Forrest S R 2009 Broad spectral response using carbon nanotube/organic semiconductor/C₆₀ photodetectors *Nano Lett.* **9** 3354–8

- [6] Bindl D J, Wu M-Y, Prehn F C and Arnold M S 2011 Efficiently harvesting excitons from electronic type-controlled semiconducting carbon nanotube films *Nano Lett.* **11** 455–60
- [7] Tune D D *et al* 2013 The role of nanotubes in carbon nanotube–silicon solar cells *Adv. Energy Mater.* **3** 1091–7
- [8] Arnold M S, Green A A, Hulvat J F, Stupp S I and Hersam M C 2006 Sorting carbon nanotubes by electronic structure using density differentiation *Nat. Nanotechnol.* **1** 60–5
- [9] Arnold M S, Stupp S I and Hersam M C 2005 Enrichment of single-walled carbon nanotubes by diameter in density gradients *Nano Lett.* **5** 713–8
- [10] Jin S H *et al* 2013 Using nanoscale thermocapillary flows to create arrays of purely semiconducting single-walled carbon nanotubes *Nat. Nanotechnol.* **8** 347–55
- [11] Ju S-Y, Doll J, Sharma I and Papadimitrakopoulos F 2008 Selection of carbon nanotubes with specific chiralities using helical assemblies of flavin mononucleotide *Nat. Nanotechnol.* **3** 356–62
- [12] Khripin C Y, Fagan J A and Zheng M 2013 Spontaneous partition of carbon nanotubes in polymer-modified aqueous phases *J. Am. Chem. Soc.* **135** 6822–5
- [13] Liu H, Nishide D, Tanaka T and Kataura H 2011 Large-scale single-chirality separation of single-walled carbon nanotubes by simple gel chromatography *Nat. Commun.* **2** 309
- [14] Nish A, Hwang J-Y, Doig J and Nicholas R J 2007 Highly selective dispersion of single-walled carbon nanotubes using aromatic polymers *Nat. Nanotechnol.* **2** 640–6
- [15] Tu X, Manohar S, Jagota A and Zheng M 2009 DNA sequence motifs for structure-specific recognition and separation of carbon nanotubes *Nature* **460** 250–3
- [16] Fagan J A, Becker M L, Chun J and Hobbie E K 2008 Length fractionation of carbon nanotubes using centrifugation *Adv. Mater.* **20** 1609–13
- [17] Ghosh S, Bachilo S M and Weisman R B 2010 Advanced sorting of single-walled carbon nanotubes by nonlinear density-gradient ultracentrifugation *Nat. Nanotechnol.* **5** 443–50
- [18] Green A, Duch M and Hersam M 2009 Isolation of single-walled carbon nanotube enantiomers by density differentiation *Nano Res.* **2** 69–77
- [19] Tyler T P, Shastry T A, Leever B J and Hersam M C 2012 Narrow diameter distributions of metallic arc discharge single-walled carbon nanotubes via dual-iteration density gradient ultracentrifugation *Adv. Mater.* **24** 4765–8
- [20] Green A A and Hersam M C 2011 Nearly single-chirality single-walled carbon nanotubes produced via orthogonal iterative density gradient ultracentrifugation *Adv. Mater.* **23** 2185–90
- [21] Zhao P, Einarsson E, Xiang R, Murakami Y and Maruyama S 2010 Controllable expansion of single-walled carbon nanotube dispersions using density gradient ultracentrifugation *J. Phys. Chem. C* **114** 4831–4
- [22] Fagan J A, Becker M L, Chun J, Nie P, Bauer B J, Simpson J R, Hight-Walker A and Hobbie E K 2008 Centrifugal length separation of carbon nanotubes *Langmuir* **24** 13880–9
- [23] Shastry T A, Morris-Cohen A J, Weiss E A and Hersam M C 2013 Probing carbon nanotube–surfactant interactions with two-dimensional DOSY NMR *J. Am. Chem. Soc.* **135** 6750–3
- [24] Nair N, Kim W-J, Braatz R D and Strano M S 2008 Dynamics of surfactant-suspended single-walled carbon nanotubes in a centrifugal field *Langmuir* **24** 1790–5
- [25] Schiebl S P, Fröhlich N, Held M, Gannott F, Schweiger M, Forster M, Scherf U and Zaumseil J 2015 Polymer-sorted semiconducting carbon nanotube networks for high-performance ambipolar field-effect transistors *ACS Appl. Mater. Inter.* **7** 682–9
- [26] Ju S-Y, Abanulo D C, Badalucco C A, Gascón J A and Papadimitrakopoulos F 2012 Handedness enantioselection of carbon nanotubes using helical assemblies of flavin mononucleotide *J. Am. Chem. Soc.* **134** 13196–9
- [27] Ju S-Y, Kopcha W P and Papadimitrakopoulos F 2009 Brightly fluorescent single-walled carbon nanotubes via an oxygen-excluding surfactant *Organization Science* **323** 1319–23
- [28] Sim J, Oh H, Koo E and Ju S-Y 2013 Effect of tight flavin mononucleotide wrapping and its binding affinity on carbon nanotube covalent reactivities *Phys. Chem. Chem. Phys.* **15** 19169–79
- [29] Oh H, Sim J and Ju S-Y 2013 Binding affinities and thermodynamics of noncovalent functionalization of carbon nanotubes with surfactants *Langmuir* **29** 11154–62
- [30] Nikolaev P, Bronikowski M J, Bradley R K, Rohmund F, Colbert D T, Smith K A and Smalley R E 1999 Gas-phase catalytic growth of single-walled carbon nanotubes from carbon monoxide *Chem. Phys. Lett.* **313** 91–7
- [31] O’Connell M J *et al* 2002 Band gap fluorescence from individual single-walled carbon nanotubes *Science* **297** 593–6
- [32] Arnold M S, Suntivich J, Stupp S I and Hersam M C 2008 Hydrodynamic characterization of surfactant encapsulated carbon nanotubes using an analytical ultracentrifuge *ACS Nano* **2** 2291–300
- [33] Fagan J A, Zheng M, Rastogi V, Simpson J R, Khripin C Y, Silvera Batista C A and Hight Walker A R 2013 Analyzing surfactant structures on length and chirality resolved (6, 5) single-wall carbon nanotubes by analytical ultracentrifugation *ACS Nano* **7** 3373–87
- [34] Tait M J, Suggett A, Franks F, Ablett S and Quickenden P A 1972 Hydration of monosaccharides: a study by dielectric and nuclear magnetic relaxation *J. Solution Chem.* **1** 131–51
- [35] Yizhak M 1988 Ionic radii in aqueous solutions *Chem. Rev.* **88** 1475–98

Supplementary information

Affinity-mediated Sorting Order Reversal of Single-Walled Carbon Nanotubes in Density Gradient Ultracentrifugation

*Myungsu Jang, Somin Kim, Haneul Jeong, and Sang-Yong Ju**

Department of Chemistry, Yonsei University, 50 Yonsei-ro, Seodaemun-Gu, Seoul 03722, Korea

* E-mail: syju@yonsei.ac.kr

Methods

FMN-HiPco suspension protocol: To maximize SWNT concentration, a mixture of 7.5 mg HiPco SWNTs and 150 mg FMN was added to 15 mL of H₂O, modified from the previously reported protocol from literature [S1, S2]. The resulting suspension was bath-sonicated for 1 hr (Branson 1510 sonicator, 70 W) and then probe-sonicated (VCX 750, probe tip diameter: 13 mm, Sonics & Materials) for 5 hr at a power level of 300 W. The resultant aqueous dispersion was ultra-centrifuged at 80,000 g for 3 hr (SW 41-Ti rotor, Beckman Coulter) and the upper 80% of the supernatant was carefully collected.

Iodixanol nonlinear density gradient preparation: An aqueous solution of iodixanol was used as density gradient medium. The nonlinear density gradient was prepared according to literature by Ghosh and co-workers [S3]. Stock solutions with various iodixanol concentrations (*i.e.*, 20.0, 21.0, 22.0, 23.5, 25.0, 26.0, 27.0, 28.5, 30.0, 35.0, 40.0, 60.0 w/v %) were prepared to produce varying density, as shown in Table S1. Density gradients were formed in a centrifuge tube (13.2 mL capacity, ultraclear thinwall tube, 14 mm × 89 mm, Beckman Coulter) by introducing discrete density layers with a blunt-needled syringe from the bottom, with a density range from 1.320 to 1.107. To create smooth density, the tube was tilted by 50 degrees from the vertical and was allowed to equilibrate by diffusion for 1 hr at room temperature. The density gradient media after ultracentrifugation was fractionated by 50.0 μL portion to measure n_D and a density profile (Figure S2) was produced using a correlation curve. Except refractive measurement, 1 mM FMN was added to each iodixanol layer to ensure nanotube stability during the centrifugation step. 0.585 mL of aqueous FMN-SWNT dispersion was premixed with 0.415 mL 60 w/v % iodixanol to produce 1.000 mL FMN-SWNT dispersion containing 25 w/v % iodixanol. A 1-mL dispersion was carefully injected immediately above the 25 w/v% density layer of iodixanol. Subsequently, the resulting centrifuge tube was centrifuged at 80,000 g for 20 hrs (SW41Ti swing-bucket rotor, Optima LE-80K ultracentrifuge, Beckman Coulter) at 22°C.

PL and PLE measurements along tube depth: Fluorescence spectroscopy measurements were conducted on a Spex Nanolog 3-211 spectrofluorometer (Horiba Jobin-Yvon) excited using a 450-W Xe lamp equipped with a liquid nitrogen-cooled, single-channel InGaAs detector. Both excitation and emission light intensities were corrected against instrumental variations using sensitivity correction factors to produce the PLE map. *PL and PLE spectra along centrifugation tube depth:* To investigate the PLE depth profile, custom-made optical components

were used to focus the excitation lights and translator, as shown in Figure S3. 3 mm horizontal kinematic slit was installed at the entrance port of beam into sample chamber. A convex lens ($f = 30$ mm, AC254-030-A-ML, Thorlabs) was inserted in the excitation path to reduce beam size from 10×8 mm² to 5×4 mm². Second, a custom-made translator on the rail was installed to the sample chamber wall. A micro positioner (LT1, Thorlabs) equipped with a tube holder was installed on the rail carrier (RC1, Thorlabs) on a rail (travel length: 1500 mm, RLA150, Thorlabs) using a ruler. Fine and coarse depth adjustment was obtained by a micrometer and rail with a ruler, respectively. PL depth profile by laser was obtained by excitation of focused laser (635 nm, 1.0 mW, Thorlabs, CPS180) by using a convex lens ($f = 300$ mm, LA1484-A, Thorlabs).

Anhydrous density calculation of FMN-(8,6): In order to calculate buoyant density of FMN-SWNTs, we utilized (8,6) nanotube which has been modeled to have optimal geometry with FMN wrapping. [S1, S2] Based on 1.42 Å C-C distance, FMN wrapping on (8,6) tube with $d_t = 0.95$ nm has δ_1 helical motif. First, r_{core} as shown in Figure 1B in the main text can be calculated as the following:

$$r_{core} = \frac{d_t \text{ of (8,6)}}{2} - \frac{\text{vdW distance (0.34 nm)}}{2} = 0.31 \text{ nm}$$

We further calculate r_{an} . Methyl group of lumiflavin (or N-methyl isoalloxazine) was removed to obtain r_{an} form (i.e., isoalloxazine-(8,6) construct, as shown in Figure S8A). The lattice parameter of the optimized hexagonal unitcell having smallest free volume is $a = c = 23.10$ Å, and $b = 25.91$ Å. This produces r_{an} to be 11.55 Å. Anhydrous density is calculated by using cylindrical model as shown in Figure S8B. Anhydrous volume is as following:

$$V = \pi(r_{an}^2 - r_{core}^2)L = \pi \{(1.155 \text{ nm})^2 - (0.305 \text{ nm})^2\} \times 2.591 \text{ nm} = 10.09 \text{ nm}^3$$

This unitcell contains 7414.9 g/mol of isoalloxazine-(8,6) construct. Based on this, $\rho_{anhydrous}$ is estimated to be 1.221 g/mL.

K_a determination by optical titration assay: K_a determination was carried out by using optical titration assay according to previously published literature.[S3, S4] Prior to collect the photoluminescence excitation (PLE) contour spectra, 1- μ L aliquot of 0.3 M aqueous SDBS solution was added to a fluorescence cuvette (10 mm path length) containing a 3-mL FMN-HiPco sample to become 0.1 mM SDBS concentration in FMN-HiPco solution. In this manner, array of PLE spectra according to SDBS concentration was measured at 18 °C. PLE spectra array was imported to generate a concentration-dependent PL intensity trace using (n, m) positions at SDBS wrapped

SWNTs utilizing Matlab software. Hill function (*i.e.*, Hill1 code) as implemented by Origin software was used for nonlinear curve fitting.

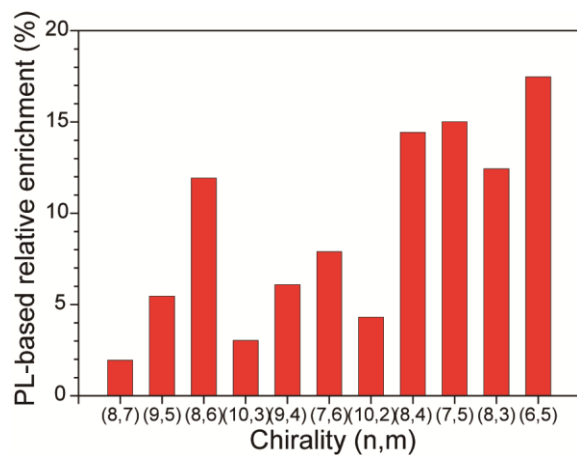


Figure S1. PLE-based abundance histogram of initial SWNT chiralities according to descending SWNT d_t .

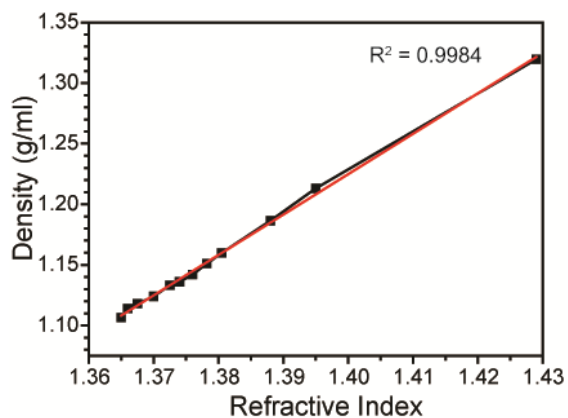


Figure S2. Correlation curve between measured refractive indices and iodixanol densities.

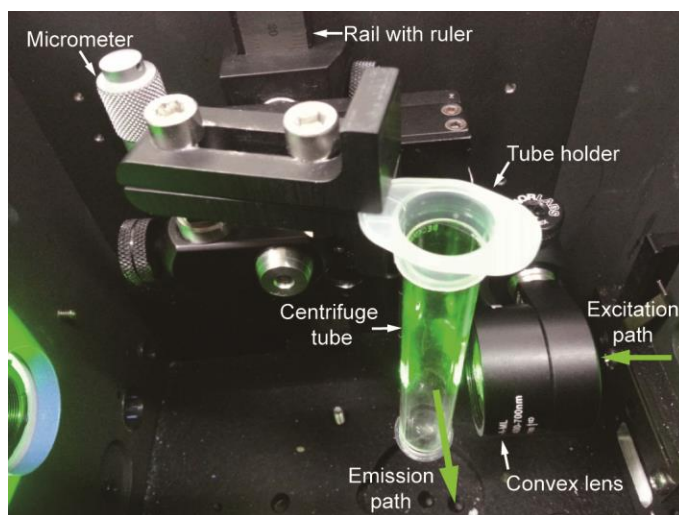


Figure S3. Photograph of custom-made translation setup used to probe PL emission along the centrifugation tube. A convex lens was placed into the excitation side while a micrometer translation stage was installed on a rail setup.

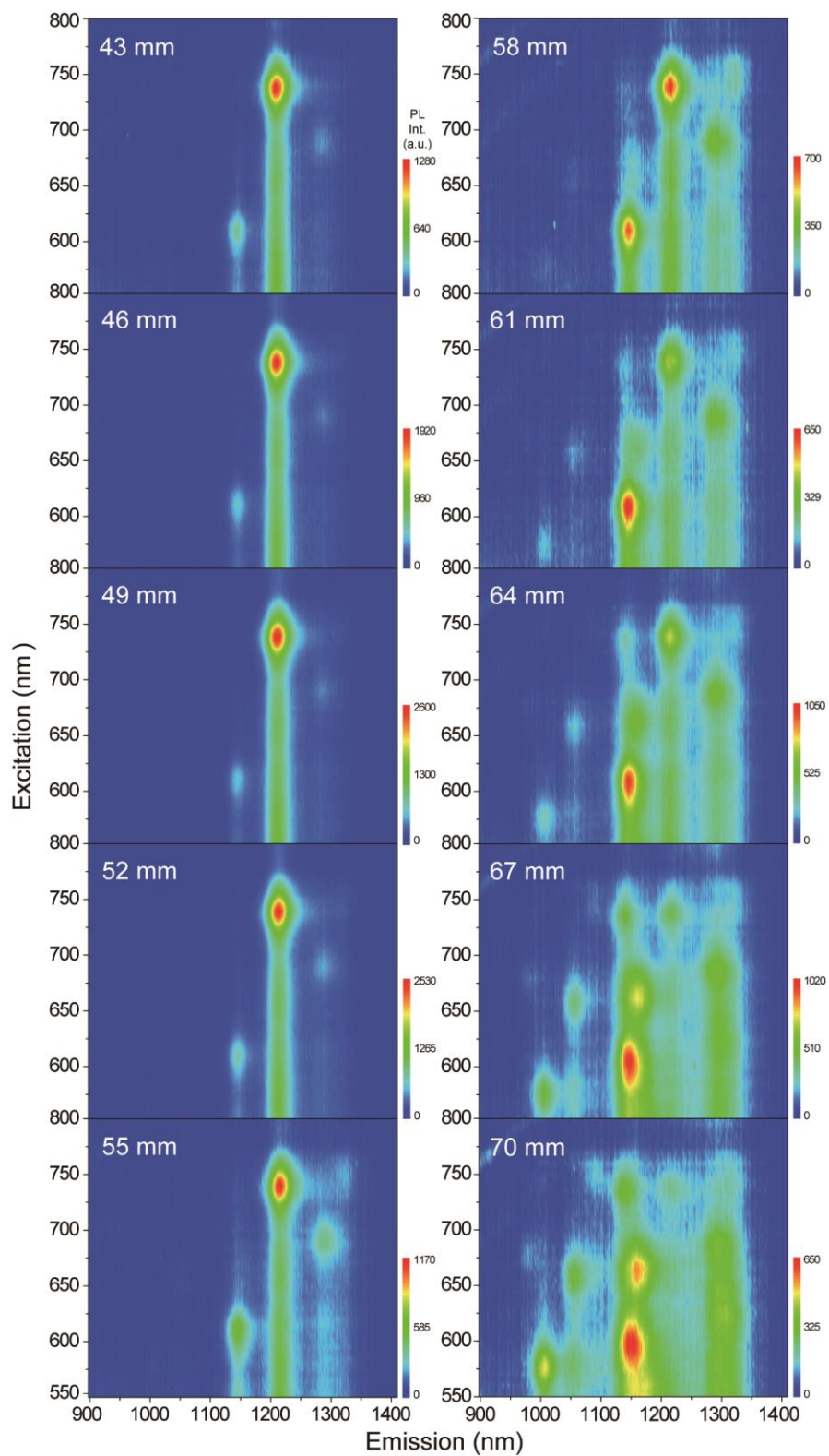


Figure S4. PLE maps obtained from each depth by 3 mm intervals. PL intensities are listed on the right.

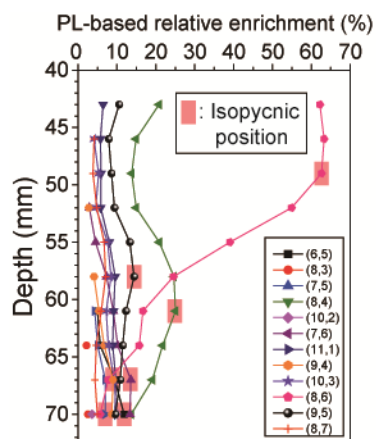


Figure S5. PLE-based enrichment and isopycnic points of SWNT chiralities along depth. Isopycnic points are indicated by colored box.

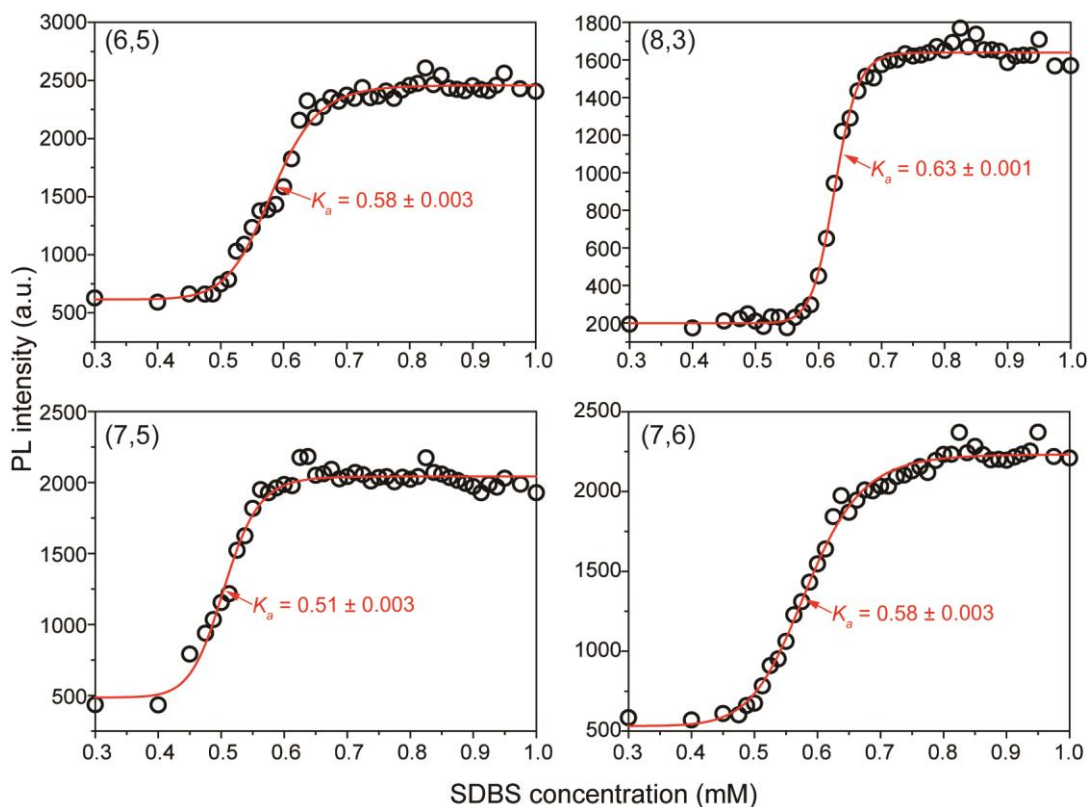


Figure S6. Additional K_a determination by titrating FMN-SWNT against SDBS according to nanotube chirality. Black and red circles indicate PL intensity from FMN- and SDBS-derived SWNTs, respectively. Solid lines are fitted using a Hill curve.

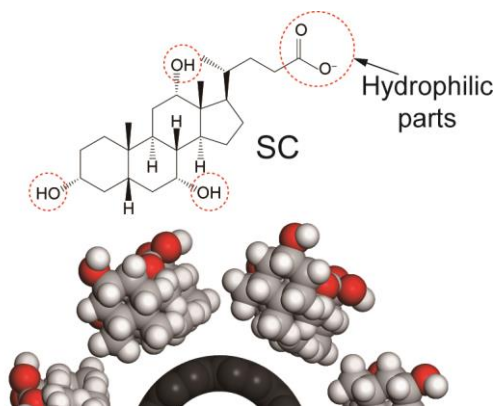


Figure S7. Schematics of SC-wrapped SWNTs. Inset display chemical structure of SC. Red, grey, and white spheres indicates O, C, and H.

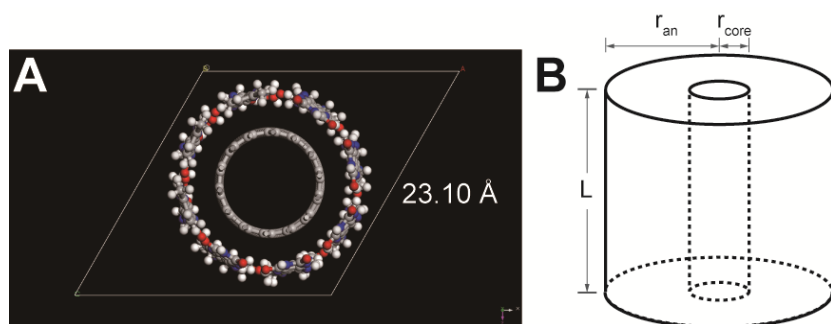


Figure S8. Anhydrous density calculation by simple geometric model. (A) Isoalloxazine-(8,6) construct in unitcell. (B) Hollow cylindrical model.

Table S1. Details of nonlinear iodixanol layering and density.

| Iodixanol content (w./v. %) | Density (g/cm ³) | Dilution (mL) | | DGU (mL) |
|--------------------------------|---------------------------------|---------------------|-------|-------------|
| | | 60 w./v.% iodixanol | Water | |
| 20.0 | 1.107 | 3.33 | 6.67 | 0.2 |
| 21.0 | 1.114 | 3.50 | 6.50 | 0.3 |
| 22.0 | 1.118 | 3.67 | 6.33 | 0.3 |
| 23.5 | 1.124 | 3.92 | 6.08 | 0.3 |
| 25.0 | 1.133 | 4.17 | 5.83 | 0.4 |
| 26.0 | 1.136 | 4.34 | 5.66 | 0.4 |
| 27.0 | 1.142 | 4.50 | 5.50 | 0.5 |
| 28.5 | 1.151 | 4.75 | 5.25 | 0.5 |
| 30.0 | 1.160 | 5.00 | 5.00 | 1.0 |
| 35.0 | 1.186 | 5.82 | 4.17 | 1.5 |
| 40.0 | 1.213 | 6.67 | 3.33 | 2.0 |
| 60.0 | 1.320 | 10.00 | 0.00 | 3.1 |

Table S2. K_a value and error bars determined by optical titration assay of FMN-SWNTs against SDBS according to SWNT chirality.

| (n,m) | Assignment | | PL position of FMN-HiPco | | | | FMN-HiPco | | |
|---------|------------|-----------------|--------------------------|-----------------|-----------------|-----------------|------------|----------------|----------|
| | d_t [nm] | Chiral Angle[°] | E_{11}^S [nm] | E_{22}^S [nm] | E_{11}^S [eV] | E_{22}^S [eV] | K_a [mM] | Error in K_a | γ |
| (6,5) | 0.75 | 27 | 1003 | 582 | 1.24 | 2.13 | 0.58 | 0.003 | 16 |
| (8,3) | 0.77 | 15.3 | 987 | 677 | 1.26 | 1.83 | 0.63 | 0.001 | 34 |
| (7,5) | 0.82 | 24.5 | 1062 | 655 | 1.17 | 1.89 | 0.51 | 0.003 | 18 |
| (8,4) | 0.83 | 19.1 | 1146 | 605 | 1.08 | 2.05 | 0.49 | 0.004 | 24 |
| | | | | | | | 0.72 | 0.003 | 29 |
| (7,6) | 0.88 | 27.5 | 1160 | 670 | 1.07 | 1.85 | 0.58 | 0.003 | 13 |
| (8,6) | 0.95 | 25.3 | 1212 | 737 | 1.02 | 1.62 | 0.68 | 0.003 | 21 |
| (9,5) | 0.96 | 20.6 | 1286 | 689 | 0.96 | 1.80 | 0.72 | 0.004 | 20 |

Cited references

- [S1] Ju S-Y, Abanulo D C, Badalucco C A, Gascón J A and Papadimitrakopoulos F 2012 Handedness Enantioselection of Carbon Nanotubes Using Helical Assemblies of Flavin Mononucleotide *J. Am. Chem. Soc.* **134** 13196-9
- [S2] Ju S-Y, Doll J, Sharma I and Papadimitrakopoulos F 2008 Selection of Carbon Nanotubes with Specific Chiralities Using Helical Assemblies of Flavin Mononucleotide *Nat. Nanotechnol.* **3** 356-62
- [S3] Ghosh S, Bachilo S M and Weisman R B 2010 Advanced Sorting of Single-Walled Carbon Nanotubes by Nonlinear Density-Gradient Ultracentrifugation *Nat. Nanotechnol.* **5** 443-50
- [S4] Oh H, Sim J and Ju S-Y 2013 Binding Affinities and Thermodynamics of Noncovalent Functionalization of Carbon Nanotubes with Surfactants *Langmuir* **29** 11154-62